Letter of Intent for Drell-Yan Measurements of Nucleon and Nuclear Structure with the FNAL Main Injector.

The E866 Collaboration
(D. F. Geesaman Spokesman for 120 GeV Measurements.)

April 15, 1998

Abstract

We propose to make precise measurements of the fractional momentum (x) distributions of the ratio of d-antiquarks to u-antiquarks in the proton, $\bar{d}/\bar{u}$, using proton induced Drell-Yan reactions at 120 GeV. Recent E866 measurements unexpectedly suggest considerable x dependence in this ratio at $x >0.2$. High intensity primary proton beams from the Main Injector make it possible to extend the x range of the E866 measurements with high precision. The apparatus will also be used to precisely measure the change in the $\bar{u}$ distributions in nuclear targets at $x >0.2$.

Contents

1 Introduction

While proton structure functions have been measured in deep inelastic scattering over ranges of five-orders-of-magnitude in both the fractional momentum of the parton, x, and the virtuality of the incident photon, Q^2, the underlying non-perturbative parton distributions must be determined by phenomenological fits e.g. [1, 2]. Each time new data have tested underlying assumptions of the phenomenology that were unconstrained by known symmetries, the phenomenology has been found wanting. For example, no known symmetry requires the equality of the $\bar{d}$ and $\bar{u}$ distributions in the proton, but, until 1991, this was a common assumption. Following the NMC observation [3] that the integral of $\bar{d} - \bar{u}$ is non-zero, NA51 [4] used the Drell-Yan process to confirm this difference and E866 [5, 6] recently measured the x dependence of $\bar{d}/\bar{u}$ and $\bar{d} - \bar{u}$ from $0.03 < x < 0.32$. The E866 results for $\bar{d}/\bar{u}$ are shown in Figure 1 along with the NA51 result and the CTEQ4M prediction [1] for this quantity.

Fundamentally, the nucleon structure functions are non-perturbative manifestations of Quantum Chromodynamics. While perturbative QCD quantitatively describes the Q^2 evolution of the parton distributions, the parton distributions themselves have not proved amenable to QCD treatment, although many *models* exist in the literature. Because first principle calculations of parton distributions have to date proven intractable, measurements of those distributions that are poorly determined provide vital information on nucleon structure which is used to constrain and refine the phenomenology. For example, the MRST [7] collaboration has already incorporated the E866 results in their new global fits yielding sea and valence distributions that differ substantially from previous parameterizations.

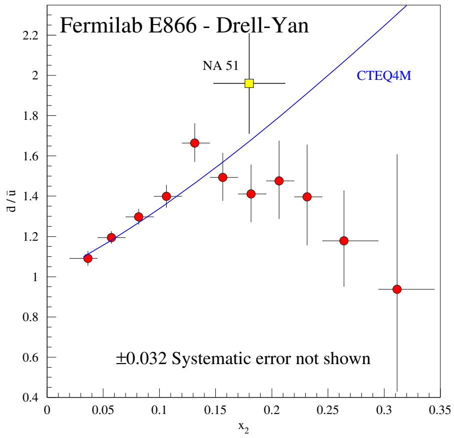

Figure 1: FNAL E866 results[5] for the x dependence of the ratio $\bar{d}/\bar{u}$ of the proton at a mass scale of 7.35 GeV. The curve represents the CTEQ4M parameterization[1]. The square is the NA51 result at a mass scale of 5.2 GeV [4]

We propose to make precise measurements of proton-induced Drell-Yan cross sections on hydrogen and deuterium. These measurements will determine $\bar{d}_p/\bar{u}_p$ for $0.1 < x < 0.5$. The measurements on deuterium are also directly sensitive to $\bar{d}_p + \bar{u}_p$ over this same range. We also propose to measure proton-induced Drell-Yan cross sections on nuclear targets. Our present knowledge of the flavor dependence of the nuclear parton distributions limits the understanding of the nuclear dependences that have been observed. (e.g. [8]). These nuclear measurements also provide a direct comparison with neutrino data on nuclear targets which are currently used to measure $\bar{d} + \bar{u}$. Our results could have implications in other areas. For example, in proton-proton collider experiments the highest energy scales are achieved via $q\bar{q}$ annihilation of large x partons. New information, especially about the flavor dependence of high x proton antiquark distributions could become important in understanding new phenomena at the LHC.

2 Physics Discussion

To lowest order, the Drell-Yan process, virtual photon production in hadron-hadron collisions, depends on the product of quark and antiquark distributions in the beam and target as:

$$\frac{d\sigma}{dx_1 dx_2} = \frac{4\pi\alpha^2}{9sx_1x_2}\sum_i e_i^2 (q_i^b(x_1,Q^2)\bar{q}_i^t(x_2,Q^2) + \bar{q}_i^b(x_1,Q^2)q_i^t(x_2,Q^2)) \tag{1}$$

where the superscripts b(t) label the beam(target) and the sum is over all quark flavors (u, d, s, c, b, t). x_1 is the fraction of the longitudinal momentum of the beam carried by the quark from the beam and x_2 is the fraction of the longitudinal momentum of the target carried by the quark from the target. The squared total energy of the beam-target system is $s = 2m_t * E_{beam} + m_b^2 + m_t^2$ with E_{beam} the energy of the beam hadron and m_b and m_t the rest masses of the beam and target hadron respectively. In the case of nuclear targets, we will assume the reaction takes place on a component nucleon, $m_t = M_n$, where M_n is the nucleon mass, and the momentum fraction is A (the number of nucleons) times the fraction of the momentum of the quark compared to the entire nucleus. The convention that c=1 is used throughout the text.

The kinematics of the virtual photon- longitudinal center of mass momentum $p_{||}^{\gamma}$, transverse momentum p_T^{γ} and mass M_γ - are determined by measuring the two-muon decay of the virtual photon. These quantities determine the momentum fractions of the two quarks:

$$x_F = p_{||}^{\gamma}/p_{||}^{\gamma,max} = x_1 - x_2 \tag{2}$$

$$x_1 x_2 s = M_\gamma^2 \tag{3}$$

where $p_{||}^{\gamma,max}$ is the maximum possible center of mass longitudinal momentum.

The kinematics are chosen to gain sensitivity to the antiquark distribution of the target with $x_F > 0$ and x_1 large so that the valence quarks of the beam dominate. In this limit the contribution from the second term in eq. (1) is small and with a proton beam the first term is dominated by the valence $u_v(x_1)$ distribution of the proton. Under these circumstances, the ratio of the cross sections for two different targets, X and Y, which have A_X and A_Y

nucleons is approximately the ratio of the $\bar{u}$ distributions:

$$\frac{\frac{1}{A_X}\frac{d\sigma^X}{dx_1 dx_2}}{\frac{1}{A_Y}\frac{d\sigma^Y}{dx_1 dx_2}} \approx \frac{\bar{u}^X(x_2)}{\bar{u}^Y(x_2)}. \tag{4}$$

In this relation the cross sections are defined per nucleus but the parton distributions are conventionally defined per nucleon.

Equation 4 demonstrates the power of Drell-Yan experiments in determining relative antiquark distributions. We wish to extend the measurements made by E866 to relatively large x_2 where the antiquark distributions are small. Beams from the FNAL Main Injector have two primary advantages compared to previous 800 GeV measurements:

- For fixed x_1 and x_2 the cross section is $\propto 1/E_{beam}$. Main Injector experiments at 120 GeV have factor of $\sim$7 larger cross sections compared to experiments with the 800 GeV Tevatron extracted beam.

- Practical limitations in the acceptable luminosity for these experiments are radiation protection limits and the singles muon rates in the detectors. To the extent that the radiation dose scales as beam power, one can take $\sim$7 times the luminosity for the same beam power at 120 GeV relative to 800 GeV. In E866 at 800 GeV, J/Ψ events from the beam dump were a significant contribution to the muon singles rates. At 120 GeV the total J/Ψ production cross sections fall by an order of magnitude when compared to 800 GeV.

We expect that the combination of these effects will allow a factor of 50 improvement in the statistics at high x_2 compared to E866 and E772.

2.1 $\bar{d}/\bar{u}$ of the proton

E866 and NA51 used measurements of the ratio of the Drell-Yan cross sections on deuterium and hydrogen to determine the ratio of $\bar{d}/\bar{u}$ on the proton by assuming the deuterium cross section is the sum of the proton and neutron cross sections and using charge symmetry to equate $\bar{d}_p$ to $\bar{u}_n$. When the antiquarks in the beam and the strange and heavier antiquarks in the target are ignored:

$$\frac{\sigma^{pd}}{2\sigma^{pp}}\Big|_{x_1>>x_2} \approx \frac{1}{2}\,\frac{(1+\frac{d(x_1)}{4u(x_1)})}{(1+\frac{d(x_1)\bar{d}(x_2)}{4u(x_1)\bar{u}(x_2)})}\left(1+\frac{\bar{d}(x_2)}{\bar{u}(x_2)}\right) \tag{5}$$

While this expression illustrates the sensitivity of the experimental ratio to $\bar{d}/\bar{u}$, the E866 extraction of $\bar{d}/\bar{u}$ was performed using eq. (1) and the CTEQ4M distributions for the valence quark distributions, the sum $\bar{d}+\bar{u}$, and the heavier sea quark distributions. The results showed little variation if MRS(R2) distributions were used. Figure 2 shows the distribution of $\bar{d}-\bar{u}$. This difference is a pure flavor non-singlet quantity: its integral is Q^2 independent [9] and its Q^2 evolution at leading order does not depend on the gluon distribution of the proton.

In perturbative QCD, differences between the $\bar{d}$ and $\bar{u}$ distributions arise only at second order and are calculated to be very small [10]. The large differences seen in Figures 1 and 2 must be non-perturbative in nature and are likely explained in terms of collective degrees of freedom of QCD at low energy. Early expectations that Pauli blocking would contribute significantly to differences in the light sea were not borne out by calculations [10]. There are three significant approaches which can accommodate large $\bar{d}-\bar{u}$ differences: 1) hadronic models of the meson cloud of the nucleon 2) chiral quark models which couple mesons directly to constituent quarks and 3) instanton models. Figure 2 illustrates calculations for representative examples of each of these models. An intriguing feature is that in each of these models the flavor and spin distributions of the proton are intimately linked.

The pion cloud model has a tantalizing simplicity and does explain basic features of the data. A proton wave function containing sizable virtual $|n\pi^+>$ Fock states will have an excess of $\bar{d}$ from the valence quarks in the π^+. If one treats the NNπ vertex function as a free parameter one can characterize the experimental distribution to x ~ 0.2 with "not-unreasonable" vertex functions (dipole vertex functions with a ~ 1 GeV cut off). The difficulty in this approach is finding justification to truncate the hadronic expansion. A more realistic inclusion of $\Delta(1232)$ isobars leads to a reduction in the predicted $\bar{d}-\bar{u}$ [11]. Again, however, with reasonable parameter choices for the $N\Delta\pi$ vertex function consistent with $pp \to p\Delta$ data, one obtains an approximate description of the $\bar{d}-\bar{u}$ data (solid curve in Figure 2). The resulting probabilities for the $|N\pi\rangle$ and $|\Delta\pi\rangle$ admixtures lead to a prediction for the difference in total spin carried by the u quarks (Δu) and the d quarks (Δd),

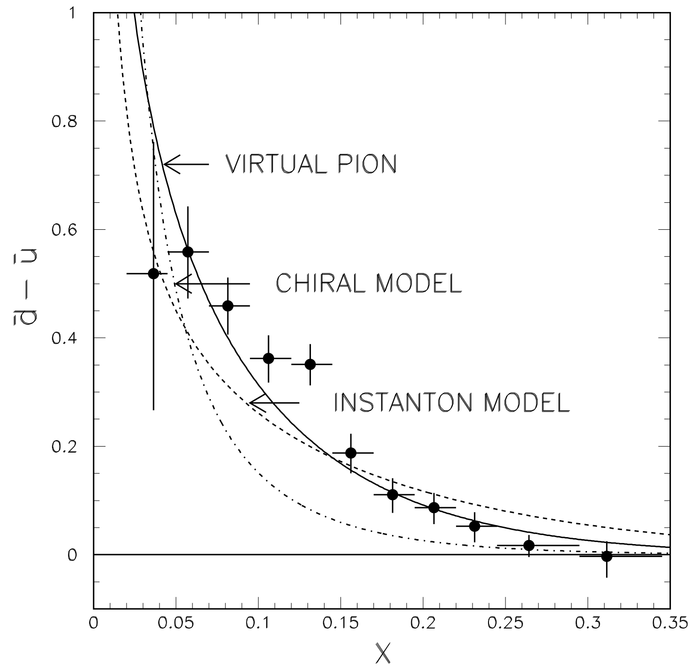

Figure 2: FNAL E866 results[6] for the x dependence of $\bar{d} - \bar{u}$ of the proton at a mass scale of 7.35 GeV. The curves represent three model calculations of $\bar{d} - \bar{u}$. The solid curve is the meson calculation including nucleons, deltas and pions [6]. The dot-dashed curve is a chiral quark model of Szczurek et al. [12] and the dashed curve is the instanton inspired parameterization of Dorokhov and Kochelev [14].

$\Delta u - \Delta d = G_A$ of 1.2 [6], close to the experimental value of $1.260 \pm .003$.

Chiral field theories suggest that the relevant degrees of freedom are constituent quarks, gluons and Goldstone bosons. Processes such as $u \rightarrow d\pi^+$ and $d \rightarrow u\pi^-$ generate a flavor asymmetry in the sea simply because there are more up than down quarks in the proton. The prediction of $\bar{d} - \bar{u}$ in one of the chiral models [12] is shown as the dot-dashed curve in Figure 2. A general feature of these models is an x dependence which is too soft because the models start with the x distribution of the valence quarks.

Instanton effective Lagrangians imply a coupling between the instantons and the valence quarks which leads to a $\bar{d} - \bar{u}$ difference. This raises the intriguing possibility that Drell-Yan measurements could provide experimental information on these theoretically very useful but seemingly experimentally inaccessible constructs. Within the framework of the t'Hooft SU(2) effective Lagrangian [13] (which is of the form $\bar{u}_R u_L \bar{d}_R d_L + \bar{u}_L u_R \bar{d}_L d_R$ where the subscripts R and L label the quark helicity) the u quarks generate a $\bar{d}d$ sea and the helicity of the valence quarks is screened [14]. (A flavor SU(3) Lagrangian would also generate $s\bar{s}$ pairs.) Dorokhov and Kochelev fit the NMC measurement of the $\bar{d} - \bar{u}$ integral to a parameterized form which is shown as the dashed curve on Figure 2. This approach also qualitatively reproduces the E866 results for x <0.23 but its only predictive power is the relations between the instanton contributions (subscript I in eq. (6)-(8)) of the spin and flavor matrix elements:

$$\begin{aligned} \bar{d}_I(x) - \bar{u}_I(x) &= -\frac{1}{4}(\Delta u_I(x) + \Delta d_I(x) + \Delta s_I(x)) && (6) \\ &= \frac{3}{5}(\Delta u_I(x) - \Delta d_I(x)) && (7) \\ &= -(\Delta u_I(x) + \Delta d_I(x) - 2\Delta s_I(x)). && (8) \end{aligned}$$

None of these models consistently incorporate the flavor symmetric sea and consequently all substantially overpredict the ratio of $\bar{d}/\bar{u}$ for x >0.23. Unfortunately the error bars on the E866 data become large in this region, due entirely to limited statistics. The pion models tend to level off at a predicted ratio $\bar{d}/\bar{u} \sim 1.5 - 5$ (depending on the baryons and mesons included in the calculations) until $x > 0.5$ where the ratio begins to decrease slowly to unity. The instanton model predicts a ratio of $\bar{d}/\bar{u} \sim 4$ at high x. One possible interpretation of the E886 results is the perturbative gluon mechanism begins to reestablish its dominance over the non-perturbative mechanisms at

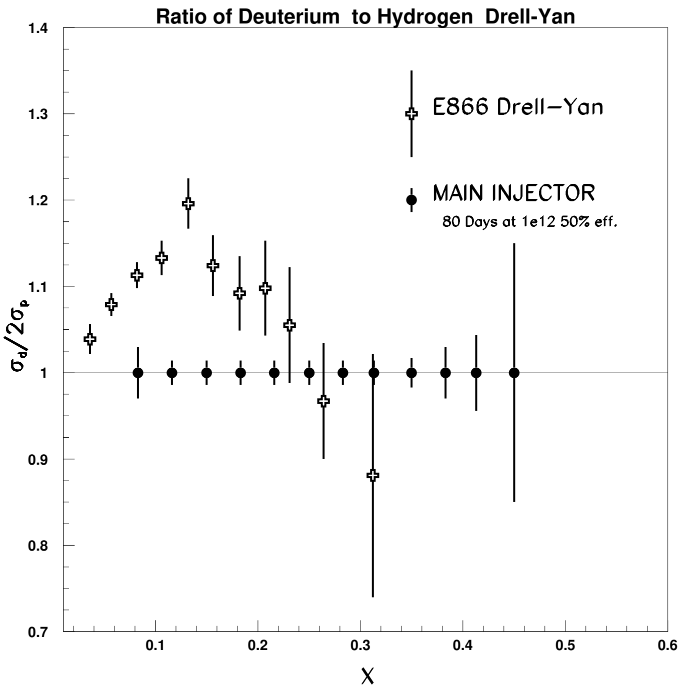

Figure 3: FNAL E866 results[5] for the x dependence of the ratio of $\sigma_d/2\sigma_p$. The statistical uncertainties expected for the measurement proposed here are shown as the error bars on the solid circles (which are arbitrarily plotted at 1.0).

a lower x value than previously expected.

The expected statistical precision with which one can measure the ratio $\frac{\sigma^{pd}}{2\sigma^{pp}}$ in an experiment at the Main Injector is shown by the error bars on the solid points in Figure 3 along with the E866 high mass results. E866 has considerably more data at spectrometer settings which emphasize lower masses, and consequently lower x_2, but this represents essentially the complete data set for large x_2. It is apparent that a high luminosity Main Injector experiment can extend the x range of our knowledge of $\bar{d}/\bar{u}$ up to $x \sim 0.5$. At even higher x values the Υ states obscure the Drell-Yan yield and make 120 GeV measurements difficult.

The cross sections on deuterium determine the flavor singlet quantity

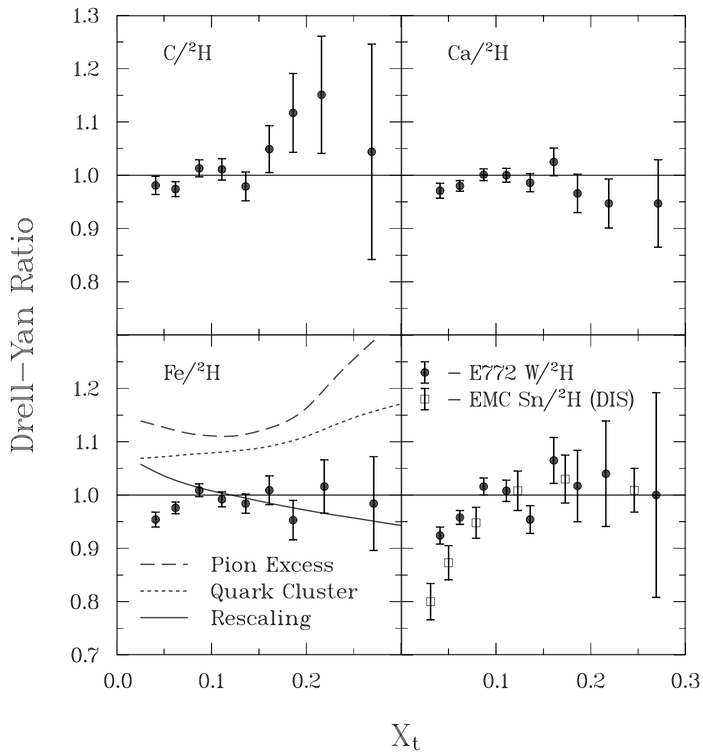

Figure 4: E772 measurements of the ratio of Drell-Yan cross sections on nuclear targets to deuterium [15].

$\bar{u}_p + \bar{d}_p$ and the extended kinematic range compared to previous measurements will be important in the global fits to determine this quantity with minimal nuclear corrections. As present, neutrino data on nuclear targets place the dominant constraints on $\bar{u} + \bar{d}$. The comparison of the nuclear dependences will be discussed in the next section.

2.2 $\bar{u}$ of Nuclei compared to $\bar{u}$ of deuterium.

In the context of nuclear convolution models, virtual pion contributions to nuclear structure functions were expected to lead to sizable increases in sea distributions of the nuclei compared to deuterium. This expectation was shattered by the convincing E772 Drell-Yan measurements [15] (See Figure 4) which showed little A dependence except in the shadowing region. High precision measurements at x larger than E772 could access would provide extremely valuable new information on the nuclear dependence of parton distributions. This information would remove any questions about the role shadowing plays in influencing the x dependence and would, for the first time, have the sensitivity to see the reduction in the nuclear sea distributions predicted in the Q^2 rescaling models. A large rise in the nuclear ratio would provide an important alert that nuclear effects may be important in the deuterium to hydrogen ratio. Figure 5 shows convolution model calculations by Coester[16] of the ratio of $\bar{u}$ in iron and deuterium to $(\bar{u} + \bar{d})/2$ of the proton and the ratio of $\bar{u}_{Fe}/\bar{u}_D$. One can observe that even in this model the predicted nuclear effects in the deuterium-to-hydrogen ratio are small for $x < 0.3$ as compared to the large effects seen in Figure 1. Since this model implies much larger nuclear effects in iron than are compatible with the E772 results, it appears to substantially overestimate the nuclear effects. By taking comparable nuclear data, we will be able to constrain the possible nuclear effects on the $\bar{d}_p - \bar{u}_p$ measurements and be able to make direct comparisons with antiquark distributions obtained from neutrino data on nuclear targets. Figure 6 illustrates a comparison of the deep inelastic and Drell-Yan results on the ratios of calcium to deuterium along with the expected errors from the measurements proposed here.

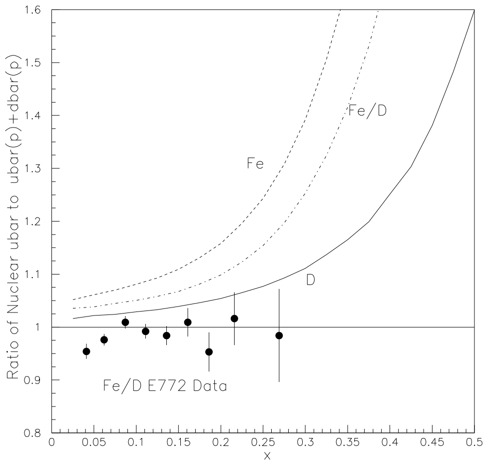

Figure 5: Ratio of $\bar{u}$ in deuterium to $(\bar{u}_p + \bar{d}_p)/2$ (solid) as calculated by Coester [16] including both nuclear motion and pion contributions. The dashed curve is the same quantity for Fe, and the dot-dashed curve is the ratio of iron to deuterium which should be directly comparable to the E772 data [15].

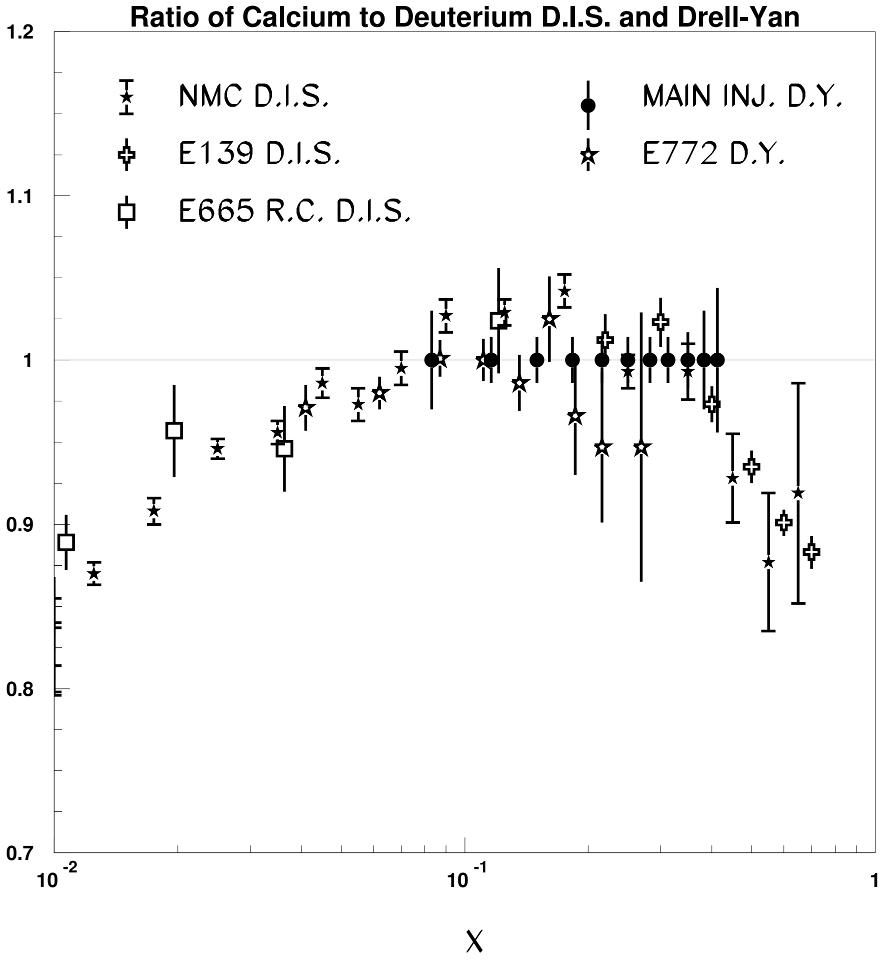

Figure 6: Compilation of deep inelastic and Drell-Yan results on the ratio of cross sections on calcium to deuterium. The statistical uncertainties expected for the measurement proposed are shown as the error bars on the solid circles (which are arbitrarily plotted at 1.0).

2.3 Interpretability of the Results

The interpretability of Drell-Yan results as direct measures of the parton distributions is based on the QCD factorization theorems [17, 18]. Bodwin, Brodsky and Lepage [18] give the condition for the minimum beam momentum P_{min} below which initial state QCD interactions become important as:

$$P_{min} \approx \frac{p_\perp A^{2/3}}{x_1} \tag{9}$$

A conservative estimate of $< p_\perp^2 > \sim 0.4$ GeV^2 (Ref. [18] use 0.25 GeV^2) yields a typical transverse hadronic scale $p_\perp$ of ~ 0.6 GeV and a minimum beam momentum of 23 GeV for $x_1 > 0.3$ and a calcium target, comfortably below the 120 GeV considered here.

2.4 Possible Future Measurements

This letter of intent focuses on measurements with the primary proton beam. A number of other interesting measurements could be made with this spectrometer. We have previously submitted a letter of intent for Drell-Yan measurements with polarized protons on a polarized proton target to determine the spin structure of the sea distributions. When a polarized proton beam becomes available from the Main Injector, the present apparatus would be immediately suitable for that experiment. Even with an unpolarized beam there appear to be interesting correlations one can measure with Drell-Yan on a polarized proton target [19]. Intense secondary meson beams would open up new possibilities such as a more accurate determination of the charged kaon valence parton distributions or measurements of the ratio of d/u distributions of the proton as $x \to 1$.

3 Experimental Apparatus

The experimental apparatus leans heavily on the E605, E772, E789 and E866 experience for the best technique to handle high luminosities in fixed target Drell-Yan experiments. The key features of the apparatus are:

- Relatively short (<15% interaction length, L_I) targets to minimize secondary reactions in the target.

- Two independent magnetic field volumes, one to focus the high transverse momentum muons and defocus low transverse momentum muons and one to measure the muon momenta.
- A 10 L_I hadron absorber to remove high transverse momentum hadrons.
- A 20 L_I beam dump at the entrance of the first magnet.
- Zinc and concrete walls for muon identification at the rear of the apparatus.

The lower beam energy has two disadvantages relative to 800 GeV experiments.

- The corresponding lower particle energies lead to increased probabilities for muon decay of the produced hadrons. This is handled by reducing the target-to-hadron-absorber distance to $\sim 1.0 - 1.5$ m.
- The lower energy muons multiple scatter more easily in the hadron absorber.

We wish to optimize the design for events with large x_2 events and $x_F \sim 0.2$. For example, the muons generated by an 8 GeV virtual photon with $x_F = 0.2$ which decays perpendicular to the direction of motion (in the virtual photon rest frame) will in the laboratory have momenta of 36 GeV, an opening angle of 200 mr and transverse momenta of 4 GeV.

A sketch of the apparatus showing trajectories for muons from 90° decays at $0 < x_F < 0.4$ is shown in Figure 7 (bend plane view) for a 7 GeV mass virtual photon. Figure 8 illustrates the non-bend plane view. A bend plane view for a J/Ψ event is shown in Figure 9.

The purpose of the first magnet of the spectrometer is to contain the high transverse momentum muons and to bend low momentum muons out of the experimental acceptance. The optimal performance would be obtained with a 3 GeV p_t kick ($\sim$ 9 T-m) large aperture magnet. Reasonable Drell-Yan acceptance is retained provided the aperture of the downstream spectrometer is large enough for field integrals as low as 5 T-m. However such a configuration increases the acceptance of low-mass pairs and hadron-decay muons resulting in unacceptably high detector count rates.

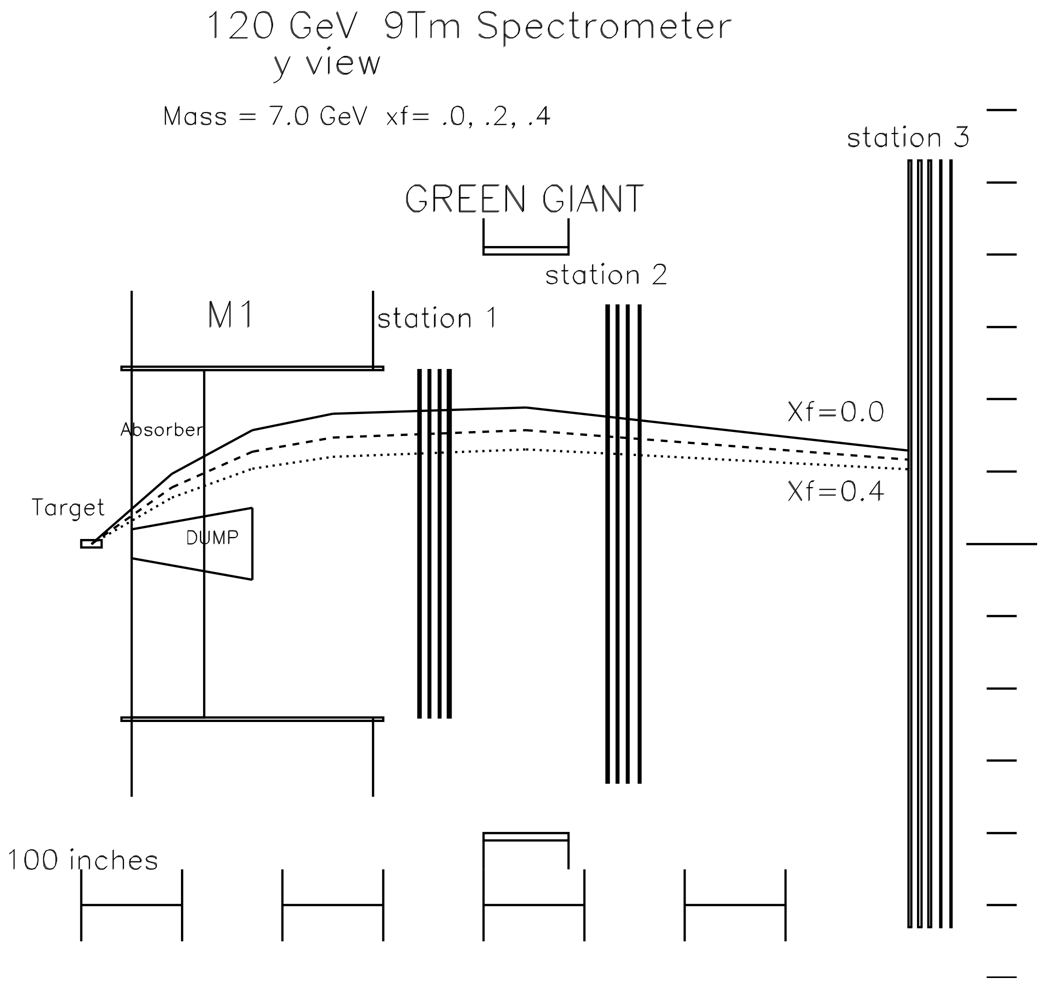

Figure 7: Bend plane view of the trajectories of one of the two muons resulting from the muon decay of a 7 GeV virtual photon (which has x_F of 0.0, 0.2 or 0.4) in a 9 T-m spectrometer.

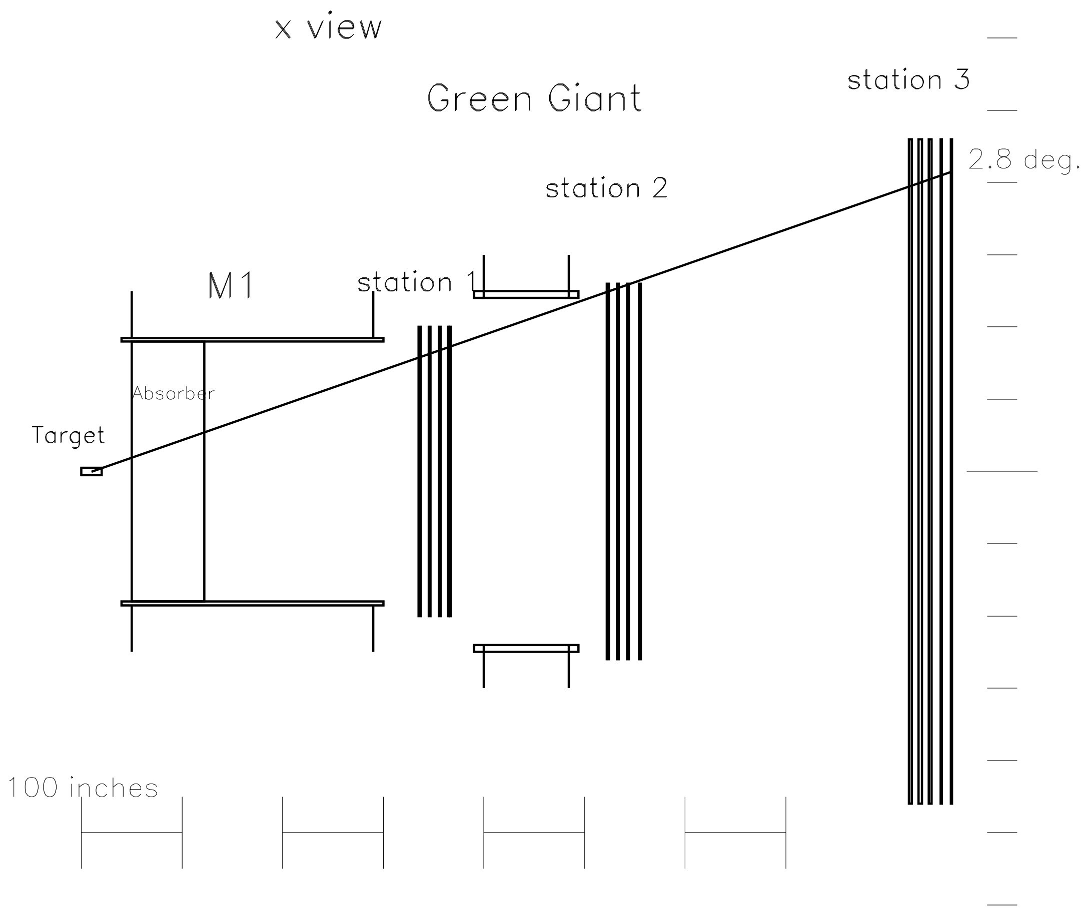

Figure 8: Non-bend plane view in a 9 T-m spectrometer. Only muons which pass around the beam dump in the bend plane contribute to the acceptance and so the beam dump is not shown.

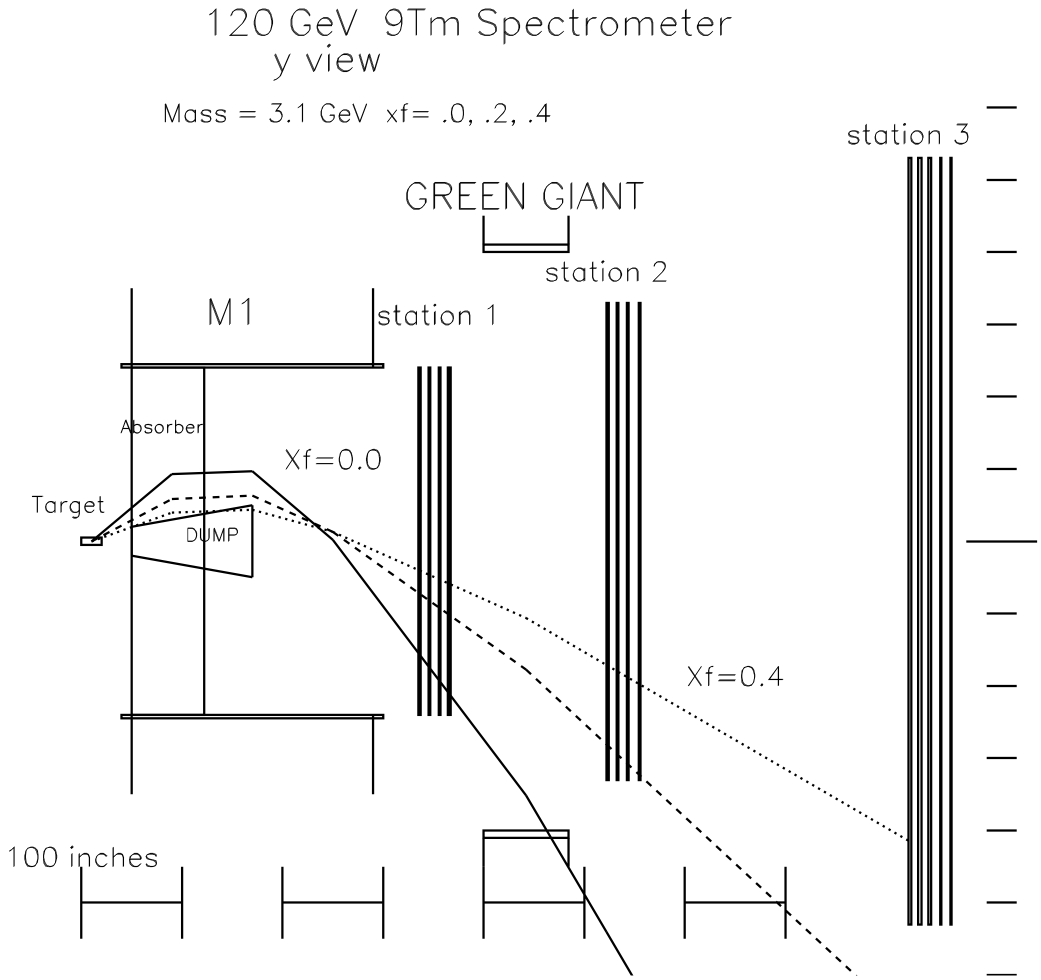

Figure 9: Bend plane view of the trajectories of one of the two muons resulting from the muon decay of a J/Ψ particle (which has x_F of 0.0, 0.2 or 0.4) in a 9 T-m spectrometer.

A 9 T-m large aperture magnet could be constructed using the iron from SM12 in Meson East with new coils, following the same principles as SM12. With such a magnet, there appear to be no experimental barriers to completing the measurement proposed here. The muons will lose ~ 3 GeV in energy passing through the absorber and multiple scatter by an average angle of $\sim 150/p_\mu$ mr. This level of multiple scattering will still permit acceptable virtual photon mass resolution ($\sim$250 MeV) and acceptable vertex resolution to separate target and beam dump events for muon energies greater than 20 GeV. Due to the long target length relative to the target-to-absorber distance, the target position does not provide additional track constraints for the mass measurement.

To reduce the cost and time scale for the experiment we are exploring the possibility of using existing magnets. To date we have not found a solution with existing magnets that can reach the required field integral and achieve acceptable singles rates in the wire chambers.

The second magnet must provide the accurate momentum determination and have a large acceptance. The existing SM3 magnet would be ideal, but is being moved to C0. The most suitable available FNAL magnet appears to be the Jolly Green Giant (JGG) which is currently in Lab G. At present, the JGG has a turn-to-turn short in one of its coils. We would need to have the short repaired to improve the p_t kick to 0.5 GeV (estimates of the cost of the repair are available).

We also expect that for radiation protection purposes, the spectrometer, like the Meson-East spectrometer, will need to be vertically bending. If so the JGG would require modification to accommodate this since it is presently configured as a horizontal bending (vertical field) magnet.

We are still in the process of studying the rate capability of the apparatus to determine the final magnet configuration. We consider this the one remaining experimental issue. We believe that a 9 T-m focusing magnet will be acceptable but have not yet determined the optimization of cost and luminosity for lower field integral concepts.

3.1 Detectors

The wire chambers and scintillators used for E866 are the appropriate size for the new spectrometer and the dimensions of these existing detectors have been used in the simulation. We would like to replace the TRANSPORT readout with a more contemporary system. We would anticipate using the same trigger strategy and trigger matrix electronics that proved successful in E866.

3.2 Muon Identification

We have also assumed the present E866 muon identification system, zinc absorber, concrete absorbers, proportional tubes and hodoscopes [20].

3.3 Yields

The experiment would use 20" long liquid hydrogen and deuterium targets, and two 10 gm/cm^2 nuclear targets and a dummy liquid target cell. The targets would be interchanged roughly every 60 minutes. Unlike the Tevatron spill with its 40 s gap between pulses, the rapid Main Injector Spills would require blocking the beam for target motion. We have assumed a primary beam intensity of 1e12 protons per pulse or 2e13 protons per minute.

Figure 10 shows the results from a Monte Carlo simulation of the acceptance of the spectrometer for the hydrogen with various acceptance cuts for 40 days at 100% efficiency running. With an 8 month run at 50% total efficiency, we would achieve these yields on four targets (hydrogen, deuterium and two nuclear targets, relative running time 44% H, 33% D, 33% nuclear) with the relative errors on the ratio of the deuterium to hydrogen cross sections for $x_F > 0.05$ shown in Figure 3.

3.4 Collaboration

The core of the collaboration, Los Alamos National Laboratory, Abilene Christian University, Texas A & M, Valparaiso and Argonne National Laboratory has recently successfully completed the E866 Drell-Yan experiment at FNAL. These groups encompass the key technologies needed for the new measurements. Several other groups have expressed interest in the experiment and we expect little problem identifying sufficient manpower to construct, operate and analyze the experiment in a timely fashion following a favorable response from FNAL.

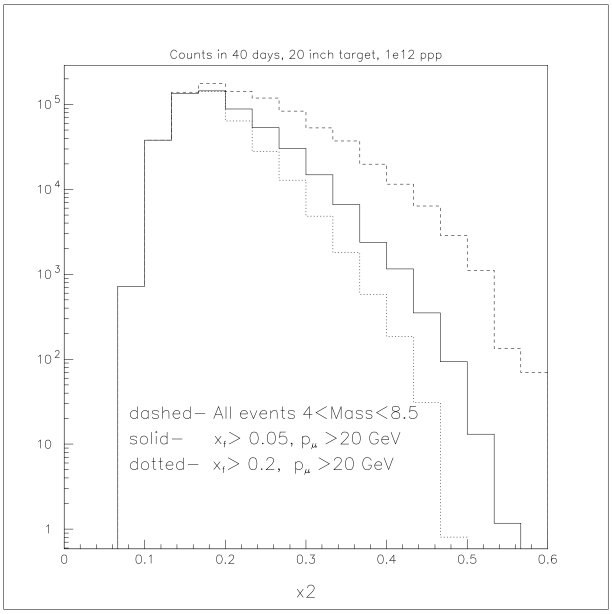

Figure 10: Monte-Carlo results for yields from a 40 day 100% efficiency run with 2e13 protons per minute on a 20" long liquid hydrogen target with the apparatus shown in Figures 7-9. The dashed curve represents all accepted events with masses between 4 and 8.5 GeV, the solid curve includes the additional requirements of: $x_F > 0.05$, and both muons having momenta greater than 20 GeV. The dotted curve includes the requirement of $x_F > 0.2$ and requires both muons to have momenta greater than 20 GeV.

4 Summary

This letter of intent proposes using the 120 GeV primary proton beam from the Main Injector to measure Drell-Yan yields for hydrogen, deuterium and two nuclear targets. These measurements will provide new information on the ratio for $\bar{d}/\bar{u}$ and $\bar{d} - \bar{u}$ distributions of the proton over the x range of 0.2-0.5 and new insight into the non-perturbative origin of the parton distributions. Measurements of the nuclear dependence of the $\bar{u}$ distribution will provide new information over a similar x range. The combination of these two measurements should also resolve nuclear ambiguities inherent in obtaining nucleon antiquark distributions from neutrino data on nuclear targets.

References

[1] H. L. Lai et al., Phys. Rev. D **55**, 1280 (1997).

[2] A. D. Martin, R. G. Roberts and W. J. Stirling, Phys. Lett. B **419**, 1280 (1997).

[3] P. Amaudruz et al., Phys. Rev. Lett. **66**, 2712 (1991); M. Arneodo at al., Phys. Rev. D **55**, R1 (1994).

[4] A. Baldit et al., Phys. Lett. B **332**, 244 (1994).

[5] E866 Collaboration, E. A. Hawker et al., to be published in Phys. Rev. Letters, 20 April 1998.

[6] E866 Collaboration, J.-C. Peng et al., submitted to Phys. Rev. Lett. (1998)

[7] A. D. Martin, R. G. Roberts, W. J. Sterling and R. S. Thorne, hep-ph/9803445.

[8] D. F. Geesaman, K. Saito and A. W. Thomas, Ann. Rev. Nucl. Part. Sci **45**, 337 (1995).

[9] A. D. Martin, W. J. Stirling and R. G. Roberts, Phys. Lett. B **252**, 653 (1990).

[10] D. A. Ross and C. T. Sachrajda, Nucl. Phys. B **149**, 497 (1979).

[11] S. Kumono, Phys. Rev. D **43**, 3067 (1991); **43**, 59 (1991); S. Kumono and J. T. Londergan, Phys. Rev. D **44**, 717, (1991).

[12] A. Szczurek et al., Nucl. Phys. A **596**, 397 (1996).

[13] G. t'Hooft, Phys. Rev. D **14**, 3432 (1976).

[14] A. E. Dorokhov and N. I. Kochelev, Phys. Lett. B **304**, 157 (1993).

[15] D. M. Alde et al., Phys. Rev. Lett. **66**, 2285 (1991).

[16] F. Coester private communication; E. T. Berger, F. Coester and R. B. Wiringa, Phys. Rev. D **29**, 398 (1984).

[17] G. T. Bodwin, Phys. Rev. D **31**, 2616 (1985); **34**, 3932 (1986).

[18] G. T. Bodwin, S. J. Brodsky and G. P. Lepage, Phys. Rev. D **39**, 3287 (1989).

[19] V. Papavassiliou, Contribution to the Main Injector Stationary Target Workshop, Fermilab, May 1997.

[20] G. Moreno et al., Phys. Rev. D **43**, 2815 (1991)